

Article

Effects of Atmospheric Turbulence on Optical Wireless Communication in NEOM Smart City

Ayshah S. Alatawi ^{1,2,*} , Albashir A. Youssef ³ , Mohamed Abaza ³ , Mohammad Ammad Uddin ² 
and Ali Mansour ⁴ 

¹ Department of Physics, Faculty of Science, University of Tabuk, Tabuk 71491, Saudi Arabia

² Sensor Networks and Cellular Systems Research Center, University of Tabuk, Tabuk 71491, Saudi Arabia; mashfaq@ut.edu.sa

³ Department of Electronics and Communication Engineering, Arab Academy for Science, Technology and Maritime Transport, Cairo 11435, Egypt; albashir.adel@aast.edu (A.A.Y.); mohamed.abaza@aast.edu (M.A.)

⁴ LabSTICC, UMR CNRS 685, ENSTA Bretagne, 29200 Brest, France; mansour@ieee.org

* Correspondence: ase.alatawi@ut.edu.sa

Abstract: The foundation of any smart city requires an innovative and robust communication infrastructure. Many research communities envision free-space optical communication (FSO) as a promising backbone technology for the services and applications provided by such cities. However, the channel through which the FSO signal travels is the atmosphere. Therefore, the FSO performance is limited by the local weather conditions. The variation in meteorological variables leads to variations of the refractive index along the transmission path. These index inhomogeneities (i.e., atmospheric turbulence) can significantly degrade the performance of FSO systems. Thus, a practical implementation of the FSO link must carefully consider the atmospheric turbulence effect. This paper aims to investigate the feasibility of FSO communication for NEOM, a promising smart city in Saudi Arabia. We study the effect of weather conditions on FSO links using the micrometeorology model, taking into account actual weather data. The FSO performance in winter and summer was compared in terms of the bit error rate, signal-to-noise ratio (SNR), link availability, and transmission distance. The study shows that the atmospheric turbulence strength is moderate and strong in winter and summer, respectively. The temperature has the biggest impact on the FSO system when compared to the other meteorological elements included in this study. Furthermore, at transmission distances less than 300 m, atmospheric turbulence does not significantly affect the FSO for the operating wavelength of 1550 nm. Furthermore, it has been shown that at transmission distances greater than 300 m, the SNR in summer is more than 18% higher than in winter. The findings of this research enable understanding of the effect of turbulence caused by NEOM weather on the FSO link, thus assisting engineers in establishing a reliable FSO backbone link by adjusting the relevant parameters.

Keywords: smart city; neom; free space optical communication; atmospheric turbulence; bit error rate (BER); scintillation



Citation: Alatawi, A.S.; Youssef, A.A.; Abaza, M.; Uddin, M.A.; Mansour, A. Effects of Atmospheric Turbulence on Optical Wireless Communication in NEOM Smart City. *Photonics* **2022**, *9*, 262. <https://doi.org/10.3390/photonics9040262>

Received: 13 March 2022

Accepted: 11 April 2022

Published: 15 April 2022

Publisher's Note: MDPI stays neutral with regard to jurisdictional claims in published maps and institutional affiliations.



Copyright: © 2022 by the authors. Licensee MDPI, Basel, Switzerland. This article is an open access article distributed under the terms and conditions of the Creative Commons Attribution (CC BY) license (<https://creativecommons.org/licenses/by/4.0/>).

1. Introduction

According to the United Nations, more than 55% of the world, population live in urban areas, and this value is expected to reach 68% by 2050 [1]. Unplanned urbanization may lead to challenges, such as depletion of natural resources, environmental degradation, and additional pressure on public services. To address these issues, the concept of smart cities has emerged [2–4].

Many countries, including the Kingdom of Saudi Arabia (KSA), have adopted smart city development as a key initiative. From 1980 to 2018, the population of Saudi Arabia increased from 9.32 million to 26.30 million, corresponding to an increase of nearly three times [5]. In addition, 90% of the areas are expected to be urbanized by 2050 [5]. These aspects are expected to introduce additional pressure on the infrastructure, including

utilities, housing, and transportation. Moreover, it may be challenging to ensure the quality of healthcare and education. To address these challenges, a smart city initiative has been announced by the Ministry of Municipal and Rural Affairs in ten cities across KSA [6]. Among these cities, the most prominent is NEOM city.

The NEOM city is unlike any other planned smart city in KSA; this city is to be built from the ground up to avoid the repetition of the standard city features. In 2017, Crown Prince Mohammed bin Salman announced the foundation of this city as a future investment. It will be located in the northern region of the Red Sea, bordering Jordan and Egypt [6].

The NEOM zone is expected to focus on nine advanced technology dimensions, including: energy, water, mobility, biotechnology, advanced manufacturing, media, entertainment, digital sciences, tourism, and sport [6,7]. Researchers have begun to explore different aspects and challenges associated with these sectors, such as the use of renewable energy and air pollution management [8–14]. The key technology to ensuring the success of any smart city is wireless technology for communication [15,16]. In August 2020, NEOM CEO Mr. N. Alnaser announced a plan to launch a center for innovation at the NEOM city to explore 5G communication aspects and its opportunities in the region [17]. The deployment of 5G across NEOM is expected to enable the incorporation of many emerging applications such as the internet of things (IoT), virtual reality, smart homes, and autonomous vehicles. In this context, wireless optical technologies such as free-space optical (FSO) have been considered, and they are promising solutions that can provide high-speed information transmission links to explore the full potential of a 5G network, realizing a speed of 100 Gbit/s or more [18–20].

The main drawback of the FSO link is that its performance is strongly dependent on local weather conditions. As the weather changes, the performance of the FSO link changes. Therefore, before deploying FSO links, it is necessary to analyze the atmospheric conditions in the region. Many researchers have investigated the performance and reliability of FSO under a variety of weather conditions in different countries [21–32]. To the best of the authors' knowledge, none of the existing studies have examined the influence of the atmospheric turbulence on the FSO communication framework recommended for use in the NEOM city. Based on the NEOM 2019 and 2020 daily meteorological data provided by the Saudi National Center for Meteorology (NCM), we investigated the effect of atmospheric turbulence on FSO link performance by using the macro-meteorological model. The result demonstrates that temperature has the greatest impact on the FSO system when compared with other meteorological components studied. Therefore, the FSO link performance in winter can be superior to that in summer. The result shows that the FSO technology is feasible under the parameters used in this study and therefore can be adopted for NEOM city.

The remaining paper is organized as follows: Section 2 illustrates the literature review. Section 3 describes the characteristics of atmospheric turbulence, and Section 4 presents the mathematical analysis. Sections 5 and 6 describe the channel models and study area, respectively. Section 7 presents the results and their discussion. The concluding remarks are presented in Section 8.

2. Literature Review

FSO communication is a promising emerging technology that can likely satisfy the requirements of next-generation networks. A general overview of FSO was presented in [33] where the author described the evolution of FSO from mirrors to telescopes to most modern wireless communication. This technology is superior to several other wireless technologies, including the microwave (radio frequency) spectrum, in terms of the high data rate, immunity from interference, high security, small size/low weight of the components, low power consumption, unlicensed spectrum, ease of use, and low cost of implementation and maintenance [16]. Moreover, problems associated with optical fiber connectivity, such as the high cost of digging paths and physical link maintenance, can be eliminated. Notably, FSO requires line-of-sight clarity to transmit data through the atmosphere channel. Thus,

the performance of the optical signal that carries the information and traverses through air degrades, largely owing to beam scattering, absorption, and atmospheric turbulence. Therefore, one of the most important elements affecting FSO link performance is the local weather. Different studies have been conducted to test optical communication under varying environments, as per the work in [34,35], mid-infrared wavelengths are found to perform well and are less affected by the environment, and its beam forming and stealth conformance make it a better choice, but it can be applied in an indoor environment. Whereas, the study [36,37] focuses mainly on the working and evaluation of FSO system under maritime environment. In [36], the authors established a model to measure the link performance by relating incident points with environment parameters. Furthermore, they conducted an experimental study to prove the performance of the proposed system. Whereas, in [37,38], the authors use both analytical and experiment studies to analyze FSO under maritime conditions. The effect of atmosphere on FSO is evident and area-specific. It is the motivation of this study to foresee the effect of NEOM weather conditions on FSO communication.

Similar studies have been conducted around the world to assess the performance of FSO links using meteorological data. Due to the frequent clear sky conditions in the Northeast of Brazil, FSO systems can provide optical communication speed and quality at a very low cost for a wavelength of $\lambda = 780 \text{ nm}$. With almost 99% availability, distances of 5 km to 8 km are possible. While 98% feasibility of FSO systems are alternatives for links with ranges up to 3.5 km and roughly 90% availability in certain cities in Brazil, southeastern and midwestern regions [21]. Rain and haze are the key limiting factors for FSO in Malaysia, according to Alama et al. [22]. Due to high bit error rate (BER) caused by seasonal heavy rain, the maximum link length is limited to 1 km for a wavelength of 1550 nm [22]. Rouissat et al. [23] attempt to identify and examine the challenges associated with FSO deployment in Algerian weather conditions. It has been determined that scintillation is one of the most significant issues in the southern region of the country, where temperatures are high almost year-round. In the North of the country, heavy rain and fog were the main problem [23]. Using data from the Libyan National Meteorological Centre, Twati et al. [24] investigated the effects of rain weather conditions on the performance of the FSO link. They found that the maximum link distance is 1.91 km under heavy rainfall weather conditions. Mohale et al. [25] investigated the viability of adopting free-space optical communication technology in six locations in South Africa. They found that, under typical conditions, Ermelo has the longest ideal FSO link distance of 7.5 km at an overall atmospheric loss of 2.8 dB, whereas Durban has the smallest optimal FSO link distance of 2.6 km at an overall atmospheric loss of 12 dB under worst-case conditions. Sultan et al. [26] studied the OFDM-FSO system performance under various weather conditions for a wavelength of 1550 nm using data from the Bangladesh Meteorological Department. They found that severe fog is the worst weather condition for the OFDM-FSO system, with a maximum feasible link of 0.4 km and a BER in the order of 10^{-3} . Under the condition of light rain, the greatest link range achievable at 40 Gbps is 3.5 km at BER in the order of 10^{-3} . In Lahore, Pakistan, Yasir et al. [27] investigate the impact of dust and rain on FSO performance for wavelength 1550 nm. Their simulation revealed that the maximal attenuations for dust and rain rate are 8.1 dB/km and 11.59 dB/km, respectively. This also indicates that FSO communication at 10Gbps across a link distance of up to 2 km is very much possible with a high SNR and a low BER. Using average meteorological measurements from the Egyptian Meteorological Unit, Algamal et al. [28] studied the performance of FSO in Alexandria, Egypt, under various weather conditions. The laser source used in this investigation had operating wavelengths of 750, 850, 950, 1310, and 1550 nm. The most difficult factors, according to the findings, were sandstorms and fog. In the presence of dense sandstorms, QAM-OFDM techniques improved the data rate by 17% when compared to standard QAM.

The effect of atmospheric turbulence on FSO systems is a considerable challenge. Such turbulence can produce beam scintillation, spreading, and wandering, resulting in a significant reduction in BER performance and the inability to use the communication link.

Using the Hufnagel Valley model, Altowij et al. [30] investigated the effect of scintillation on the performance of FSO lines in Yemen for wavelengths of 850, 1000, and 1550 nm. The report concluded that the FSO system performed admirably during the harshest conditions in Yemen. In addition, to achieve a BER of 10^{-9} utilizing the wavelength of 1550 nm during air turbulence, the distance between transmitter and receiver should be 2600 m. The effects of turbulence and refractive index fluctuation owing to temperature and pressure were investigated experimentally under different weather conditions in Pakistan [31], for an 8 GB data FSO data link over propagation distances ranging from 100 to 1500 m and 980 nm operation wavelength. It has been discovered that Pakistan, south region, is particularly ideal because it is naturally free of the majority of channel impairments that reduce the performance of traditional FSO links. This is because changes in temperature are very minor, and the refractive index that results is suitable for transmission [31]. Based on data from the Tanzania Meteorological Agency (TMA), the author of [32] explores the effect of scintillation on FSO in the two Tanzanian cities of Dar es Salaam and Dodoma. The attenuation due to scintillation was calculated using the Hufnagel Valley and Rytov models for wavelengths of 1550 nm. Dar es Salaam has a larger FSO attenuation than Dodoma, according to the case study. It has also been established that the weather conditions in Dodoma are better for FSO communication than those in Dar es Salaam. The study characteristics reveal that one can transmit over a distance of 8 km for Dar es Salaam and more than 12 km for Dodoma. According to a comparison of the two-modulation technique, non-return-to-zero (NRZ) and return to zero (RZ), NRZ is the best modulation scheme for the two cities, while October is the best month for transmission in Dodoma [32].

According to the literature reviewed, a weather analysis of the deployment location, NEOM, is required before the installation of FSO connections to help in determining the system parameters of the FSO system to achieve the desired link performance.

3. Atmospheric Turbulence

Clear air turbulence can significantly affect the transmitted optical beam. Wind and solar heat can lead to inhomogeneities in the temperature and pressure of air. These variations cause random refractive index fluctuations in the atmosphere, leading to the formation of air cells (eddies) of varying sizes and refractive indexes. Variations in the refractive index and propagation path of the optical beam in air can lead to random fluctuations in both the amplitudes and received signal phase. The block diagram of an FSO communications system is shown in Figure 1. The information signal (analog or digital) is delivered through the atmosphere using an optical transmitter. At the receiver end, the optical beam concentrates towards the photodetector, whose output is electrically processed to receive the information signal. The atmospheric turbulence effect on the optical signal depends on the size of the turbulence cell, which can be defined as follows [39]:

1. When the turbulence cells' diameters are smaller than the laser beam diameter, the laser beam bends and becomes distorted. Small differences in the arrival times of various components of the beam wavefront cause constructive and destructive interference, resulting in temporal variations in the laser beam intensity at the receiver. This effect is known as scintillation, Figure 1a.
2. If the size of the air turbulence cell is larger than the beam diameter, it can bend the optical path. Figure 1b shows how the beams (solid rays) leaving the laser source are deflected as they go through the large air cell, arriving off-axis rather than on-axis as expected in the absence of turbulence.

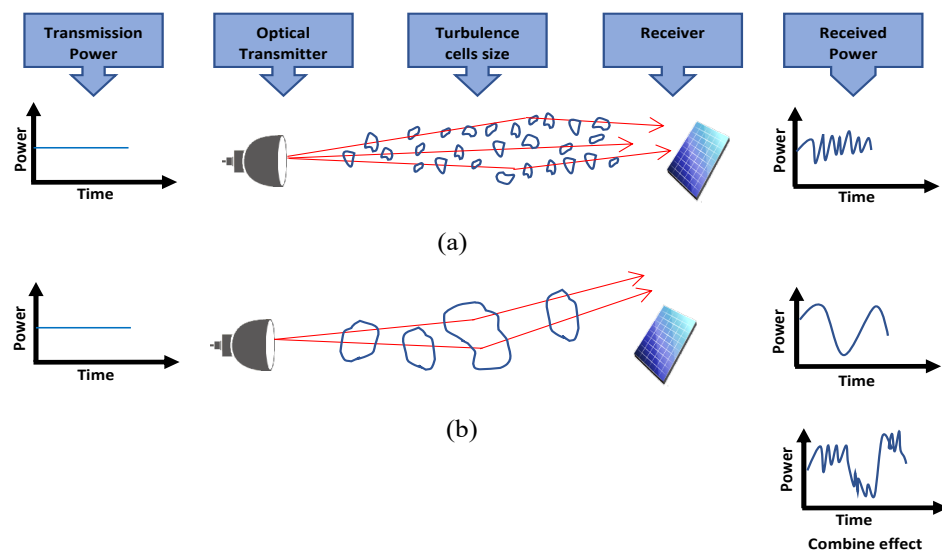


Figure 1. Comparison of Turbulent Cell Size with (a) Scintillation and (b) Beam Wander.

4. Mathematical Analysis of Atmospheric Turbulence

4.1. Refractive Index Structure Parameter

To determine the strength of atmospheric turbulence, the key aspect is the refractive index of the air, (C_n^2). However, the estimation of C_n^2 is an intensive process, owing to the specific hardware and high computation costs involved in this process [40]. Several models, such as the Hufnagel, Åi-Valley, and Greenwood models are commonly used to predict the refractive index. However, these models are appropriate over a vertical path only [40,41]. Moreover, the atmospheric turbulence varies with height and local conditions, such as the terrain type, geographical location, and meteorological values [42,43]. Consequently, it is essential to establish and enhance the C_n^2 prediction models using meteorological parameters, such as the temperature, humidity, and wind speed. In this study, we adopt a macro-meteorological model to estimate C_n^2 for the following reasons:

- The existing studies demonstrated that the macro-meteorological model can be successfully used to estimate the values of C_n^2 in a coastal area with a high correlation (up to 90%) compared with the measured values [43–47];
- This model has been validated for a similar coastal area called Negev area, as shown in Figure 2. Negev is approximately 400 km from the study area, NEOM, and has a similar landscape;
- This model can help correlate the changes in the atmospheric turbulence strength C_n^2 with the meteorological parameters.

The macro-meteorological model can be mathematically expressed as [48]:

$$C_n^2 = 3.8 \times 10^{-14}W + f(T) + f(v) + f(H) - 5.3 \times 10^{-13} \tag{1}$$

$$f(T) = 2 \times 10^{-15}T \tag{2}$$

$$f(v) = -2.5 \times 10^{-15}v + 1.2 \times 10^{-15}v^2 - 8.5 \times 10^{-17}v^3 \tag{3}$$

$$f(H) = -2.8 \times 10^{-15}H + 2.9 \times 10^{-17}H^2 - 1.1 \times 10^{-19}H^3 \tag{4}$$

where W is the weight function, T is the air temperature ($^{\circ}$ K), H is the relative humidity (%), and v is the wind speed (m/s). This model is valid under specific limits of macroscale parameters, specifically, the temperature (from 9 to 35 $^{\circ}$ C), relative humidity (from 14% to 92%), and wind speed (from 0 to 10 m/s) [48]. The weight function W is calculated based on a temporal hour that relates the actual time to sunrise and sunset, as indicated in Table 1.

$$H_T = 12 \frac{H_{actual} - H_{sunrise}}{H_{sunset} - H_{sunrise}} \tag{5}$$

where H_T is the temporal hour, H_{actual} is the actual time, $H_{sunrise}$ is the sunrise time and H_{sunset} the sunset time. The typical values of C_n^2 are $C_n^2 = 0.5 \times 10^{-14} \text{ m}^{-2/3}$ for weak turbulence, $C_n^2 = 2 \times 10^{-14} \text{ m}^{-2/3}$ for moderate turbulence, and $C_n^2 = 5 \times 10^{-14} \text{ m}^{-2/3}$ for strong turbulence [49,50].

Table 1. Weight Function [48].

Temporal Hour Interval	W	Temporal Hour Interval	W
Until -4	0.11	5 to 6	1.00
-4 to -3	0.11	6 to 7	0.90
-3 to -2	0.07	7 to 8	0.80
-2 to -1	0.08	8 to 9	0.59
-1 to 0	0.06	9 to 10	0.32
Sunrise 0 to 1	0.05	10 to 11	0.22
1 to 2	0.10	11 to 12	0.10
2 to 3	0.51	12 to 13	0.08
3 to 4	0.75	Over 13	0.13
4 to 5	0.95		



Figure 2. Map of Saudi Arabia with the NEOM City Location Marked [51].

4.2. Scintillation

Scintillation is described as the temporal and spatial fluctuation of the light intensity caused by atmospheric turbulence. The scintillation index, σ_I^2 , is defined as the normalized variance of the light wave intensity:

$$\sigma_I^2 = \frac{\langle I^2 \rangle - \langle I \rangle^2}{\langle I \rangle^2} \tag{6}$$

where I is a time series of intensity measurements, and the angle brackets denote a time average. The relation between the refractive index structure parameter and σ_I^2 is [52]

$$\sigma_I^2 = 1.23 C_n^2 k^7 L^{\frac{11}{6}} \tag{7}$$

where $k = 2\pi/\lambda$ represents the wave number, λ is the wavelength, and L is the transmission distance. The scintillation index is commonly used to classify intensity fluctuation, and its values for weak, moderate, and strong fluctuations are $\sigma_I < 1$, $\sigma_I \sim 1$, and $\sigma_I > 1$, respectively [52]. Generally, scintillation can result in a high BER.

4.3. Beam Spreading

When a beam propagates through the turbulent atmosphere, beam spreading which is defined as the broadening of the beam at the receiver surface beyond vacuum diffraction, occurs. In this section, we describe the Gaussian beam spreading of a beam propagating through turbulence at a distance L from the source. To estimate the amount of beam spreading, the effective average beam waist, $w_{eff}(L)$, is defined as follows [39]:

$$w_{eff}(L)^2 = w(L)^2 \left[1 + 1.33\sigma_I^2 \left[\frac{2L}{kw(L)^2} \right]^{\frac{5}{6}} \right] \tag{8}$$

where $w(L)$ is the beam waist at a propagation distance L .

$$w(L)^2 = w_0^2 + \left(\frac{2L}{kw_0} \right)^2 \tag{9}$$

where w_0 is the initial beam waist at $L = 0$ m.

5. Channel Model and BER Analysis

The probability density functions (PDFs) of log-normal (LN) and gamma–gamma (G-G) distributions are considered to model the turbulence [53,54]. These two models are discussed in the following sections.

5.1. LN Channel

When a channel is affected by a weak-moderate turbulence, it can be modeled using the LN. The PDF of LN channels can be defined as [53]:

$$f_h(h) = \frac{1}{2h\sigma\sqrt{2\pi}} \exp\left(-\frac{(\ln(h) - 2\mu)^2}{8\sigma^2}\right), \tag{10}$$

where $h = \exp(2X)$ is the channel irradiance from the transmitter to the receiver, with X modeled as an identically distributed Gaussian random variable with a mean μ and a variance σ^2 . The average BER (P_e) for a M-ary pulse amplitude modulation (M-ary PAM) over a LN channel can be defined as [55]

$$P_e \approx \frac{G}{12} \sum_{i=1}^n w_i \exp\left(-\frac{\log_2(M)a\bar{\gamma}e^{-4\sigma^2+x_i\sqrt{32\sigma^2}}}{4(M-1)^2}\right) + \frac{G}{4} \sum_{i=1}^n w_i \exp\left(-\frac{\log_2(M)a\bar{\gamma}e^{-4\sigma^2+x_i4\sigma\sqrt{2}}}{3(M-1)^2}\right) \tag{11}$$

where $G = \frac{2(M-1)}{M\log_2(M)\sqrt{\pi}}$, x_i and w_i are the zeros and weights of the Hermite polynomial [56] of order n , respectively. An existing study [57] demonstrated that accurate results can be obtained when $n \geq 20$ and $\bar{\gamma}$ is the average SNR, with $a = (w(L)/w_{eff}(L))^2$ where a is the loss at the beam center.

The outage probability of the proposed system over log-normal channel can be calculated using [58]

$$P_{out} = Q\left(\frac{\ln(\sqrt{a}P_M) + 2\mu}{2\sigma}\right). \tag{12}$$

where $P_M = \sqrt{\frac{\bar{\gamma}}{\gamma_{th}}}$ is the power margin and γ_{th} is the minimum signal-to-noise ratio required for no outage to occur and the signal can be decoded with an arbitrarily low error probability at the receiver.

The availability of the system can be calculated as follows

$$Availability(\%) = (1 - P_{out}) \times 100. \tag{13}$$

5.2. G-G Channel

The G-G distribution is used to model an optical channel with strong turbulence. The PDF of G-G channels can be defined as [59]

$$f_h(h) = \frac{(\alpha\beta)^{\frac{\alpha+\beta}{2}}}{\Gamma(\alpha)\Gamma(\beta)} h^{\frac{\alpha+\beta}{2}-1} G_{0,2}^{2,0} \left(\alpha\beta h \left| \begin{matrix} \cdot \\ \frac{\alpha-\beta}{2}, \frac{\beta-\alpha}{2} \end{matrix} \right. \right), \tag{14}$$

where $G_{p,q}^{m,n}[\cdot]$ is the Meijer G-function, $\Gamma(\cdot)$ is the Gamma function, and α and β are the effective number of large-scale and small-scale eddies, respectively. The corresponding values for a plane wave are as follows:

$$\alpha = \left[\exp \left(\frac{0.49\sigma_I^2}{(1 + 1.11\sigma_I^{\frac{12}{5}})^{\frac{7}{6}}} \right) - 1 \right]^{-1} \tag{15}$$

$$\beta = \left[\exp \left(\frac{0.5\sigma_I^2}{(1 + 0.69\sigma_I^{\frac{12}{5}})^{\frac{5}{6}}} \right) - 1 \right]^{-1} \tag{16}$$

The average BER for FSO communication system with a G-G channel can be expressed as [59]:

$$P_e = \frac{2^{\alpha+\beta-3}}{\pi^{\frac{3}{2}}\Gamma(\alpha)\Gamma(\beta)} G_{5,2}^{2,4} \left(a \frac{4\bar{\gamma}}{(\alpha\beta)^2} \left| \begin{matrix} \frac{2-\alpha}{2}, \frac{1-\alpha}{2}, \frac{2-\beta}{2}, \frac{1-\beta}{2} \\ 0, \frac{1}{2} \end{matrix} \right. , 1 \right) \tag{17}$$

The outage probability of the proposed system over the gamma-gamma channel can be calculated using [60]

$$P_{out} = \frac{1}{\Gamma(\alpha)\Gamma(\beta)} \times G_{1,3}^{2,1} \left[\frac{\alpha\beta}{\sqrt{a}P_M} \left| \begin{matrix} 1 \\ \alpha, \beta, 0 \end{matrix} \right. \right]. \tag{18}$$

The availability of the system can be calculated using (13).

6. Study Area: NEOM Smart City

6.1. Geographical Location

The geographical area under investigation is NEOM city. This city is located in the Tabuk region, in northwestern Saudi Arabia, close to the Jordan and Egypt borders and centered at 28°13.2' N, 34°53.3' E, as shown in Figure 2 [7]. The town's beaches extend more than 460 km over the Red Sea coast, are met by many islands, and the area contains mountains overlooking the Gulf of Aqaba and the Red Sea [7]. This location is climatically different from the remaining desert area. One of the critical characteristics of NEOM city is its geographical diversity, including both mountain ranges and sandy beaches. Thus, the city has both mountain and coastal environments.

6.2. Meteorological Information

According to the data provided by Saudi National Center for Meteorology (NCM), the NEOM climate is generally mild in the winter and hot in summer. In this study, we investigated the effect of extreme weather conditions on the FSO link in winter (December

to February) and summer (May to August) when the temperature approaches the minimum and maximum values, respectively, in the region. It is considered that owing to the moderate weather conditions in the other two seasons (spring and autumn), the FSO system will not encounter severe challenges in realizing optimal functionality. In the winter season, the monthly average temperature ranges from 16.56 °C to 21.70 °C, and the total average temperature is 18.88 °C. The summer season starts with a monthly average temperature of 30.15 °C, with an average temperature of up to 32.49 °C in the subsequent months, and the observed total average temperature is 31.79 °C, as shown in Figure 3a. Moreover, at the start of the winter season, the average humidity is 37.85%, which increases to up to 46.4% in the subsequent months. The overall average humidity is 41.9%. The humidity does not deviate significantly in the summer season: the average value ranges from 33.14% to 49.26%, and the overall average humidity is 41.49%, as shown in Figure 3b. In winter, the wind speed ranges from 4 m/s to 5 m/s, and the average value is 4.6 m/s. The oscillation of the wind speed is minimal in the summer season, and it ranges from 3.5 m/s to 3.8 m/s, with an average value of 3.8 m/s, as shown in Figure 3c. In general, the climate of NEOM is mostly stable throughout the year, unlike the dry and extremely hot weather experienced in the rest of Saudi Arabia. In particular, the overall temperature of this area is approximately 10 °C lower than the rest of the country [6].

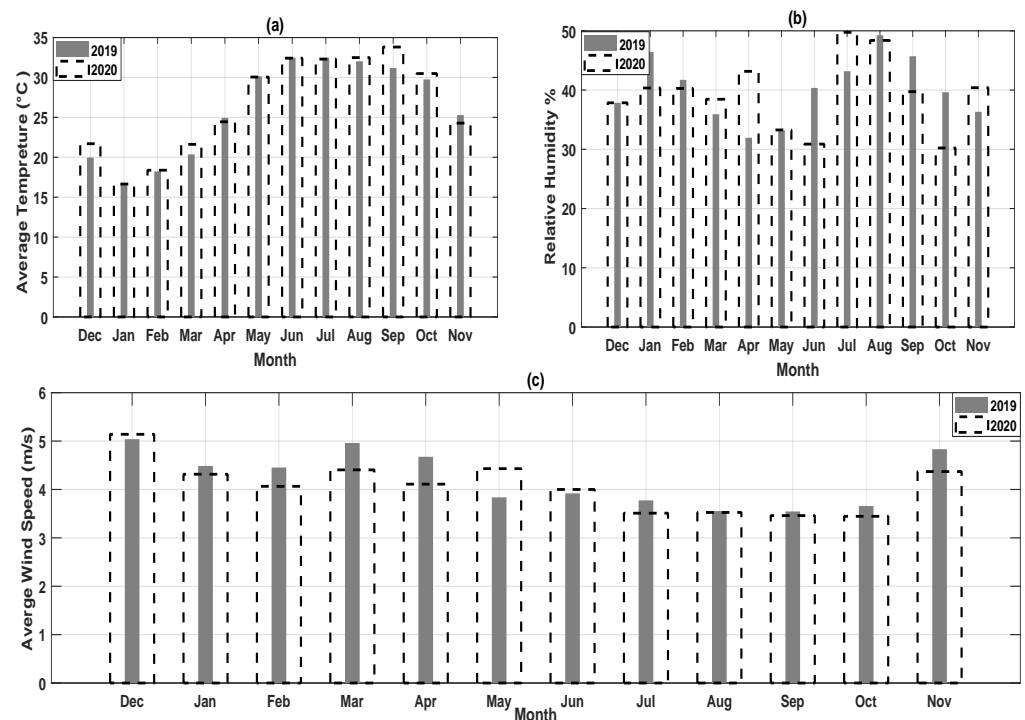


Figure 3. (a) Monthly Average Temperature, (b) Monthly Average Humidity, and (c) Monthly Average Wind Speed.

7. Results and Discussion

All attenuation sources were neglected to focus on the effect of the atmospheric turbulence on the FSO link for NEOM city. The simulations are maintained with computer capabilities: processor Intel(R) Core(TM) i7-7500U CPU @ 2.90 GHz and 8.00 GB RAM, with sample number used in simulations— 10^7 .

Using Equations (1)–(5), the refractive index structure parameter was calculated for every month. The monthly average meteorological data, T , H , and v , plotted in Figure 3, were used for this calculation. Figure 4 shows the monthly variation in the refractive index for the study years. The results indicate that the strength of the atmospheric turbulence is moderate and high in winter and summer, respectively, as indicated in Table 2.

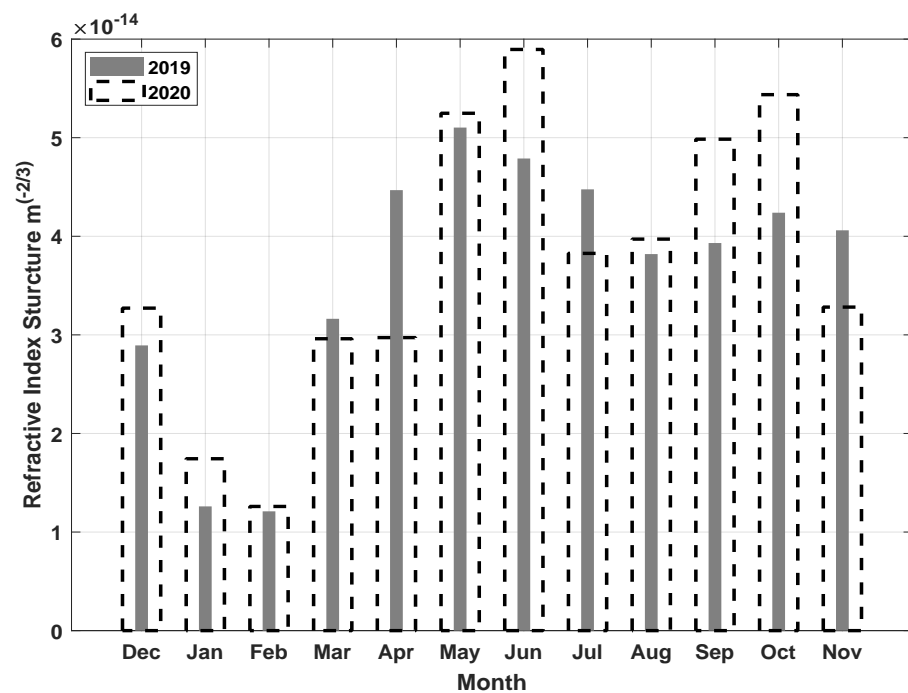


Figure 4. Month-wise Variation in C_n^2 Under the Influence of Weather Conditions.

The effects of NEOM meteorological parameters, including the temperature, wind speed, and humidity, on the turbulence strength in both seasons can be summarized as follows:

- In 2019, as shown in Figure 4, the C_n^2 peak occurred in the summer season (May), in which the temperature was high ($T = 30.42$ °C) and relative humidity was low ($H = 33.14\%$). The minimum C_n^2 value occurred in the winter season (February), in which the temperature was low ($T = 18.24$ °C) and humidity was high ($H = 46.4\%$). The results indicated that the increase in the temperature can affect the atmospheric turbulence strength more than the increase in humidity. This agrees with the experimental result of the author [61].
- As mentioned previously, in the summer season, the wind speed did not vary significantly. In the winter season, the maximum C_n^2 occurred in December for both years in which the wind speed was high (up to $\sim v = 5$ m/s). Moreover, December was the hottest month among the winter months. This finding indicates that the turbulence strength increases with the increasing wind speed and temperature in the winter season, as shown in Figure 5.

The above-mentioned findings highlight that the higher temperatures lead to strong turbulence in the summer season, and the high wind speed leads to moderate turbulence in the winter season.

Table 2. Result Calculation of Refractive Index Structure Parameter.

Season	Year	C_n^2		Turbulence Strength
		Min $\times 10^{-14}$	Max $\times 10^{-14}$	
Winter	2019	1.21	2.89	Moderate
	2020	1.26	3.42	
Summer	2019	3.82	5.1	High
	2020	4.96	5.9	

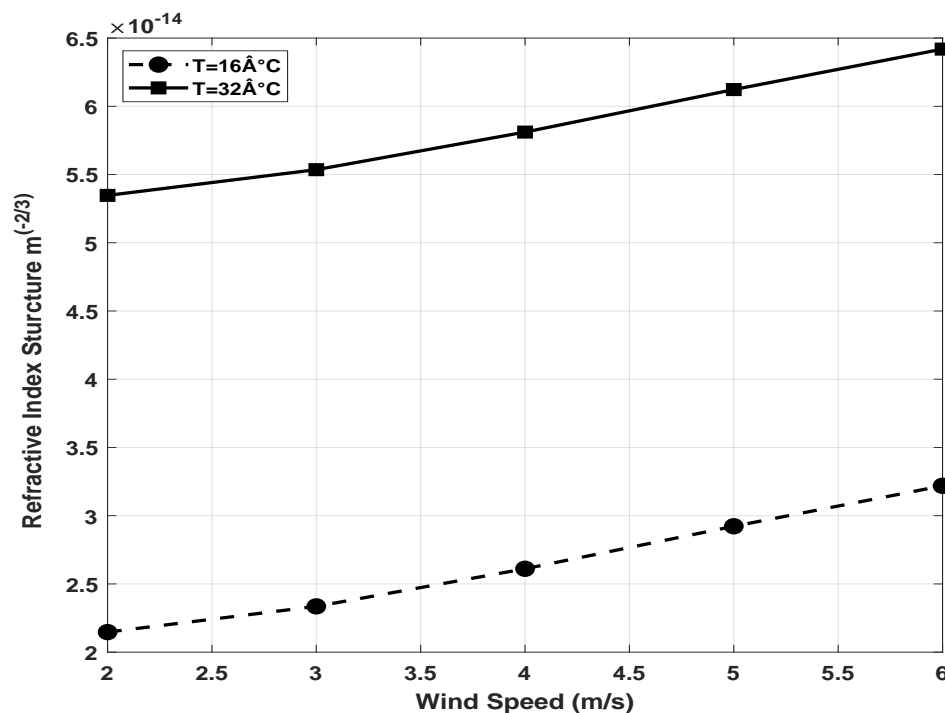


Figure 5. Variation in the Refractive Index Structure with the Wind Speed and Temperature.

Figure 6 shows the scintillation index values calculated using Equation (7). In the calculation, we considered the transmission distance as (1 km). The month-wise variation in the scintillation index under wavelengths ranging from 532 to 1550 nm was examined. The scintillation index and wavelength are inversely proportional. For example, in June, the scintillation index σ_I^2 decreased from 4.087 to 1.75 as the wavelength increased from 532 to 1550 nm. The intensity fluctuation depends on the wavelength. Moreover, the results highlight that at a wavelength of 1550 nm, the effect of atmospheric turbulence on the FSO system in NEOM city can be reduced. This result is inconsistent with the works in [30,62]. Furthermore, the scintillation is higher in summer than that in winter. For example, for $\lambda = 1550$ nm, the scintillation values in June and December are $\sigma_I^2 = 1.174$ and $\sigma_I^2 = 0.65$, respectively. The results obtained are in agreement with the experimental work in [63], which showed the increase of scintillation with increasing of temperature for the wavelength of 632 nm. For example at $T = 25$ °C and $T = 30$ °C, the scintillation $\sigma_I^2 = 1.4$ and $\sigma_I^2 = 2.1$ respectively. This result is twice the value we obtain for the same meteorological parameters for November and June, as the wavelength we used is 1550 nm.

Figure 7 shows the variation in the beam spreading at different transmission distances for $\lambda = 1550$ nm. This value of the wavelength was selected owing to the corresponding resilience to atmospheric turbulence. The range of beam spreading was calculated using Equation (8), the maximum σ_I^2 in summer (June), and minimum value in winter (February). Figure 7 shows a comparison of the beam spreading in strong turbulence during summer, moderate turbulence during winter, and in a scenario without turbulence. The higher scintillation in summer leads to approximately 28% higher beam spreading than that in the winter season. This shows the effect of temperature on the beam spreading, which agrees with the results in [63].

Furthermore, the spot size of the beam depends on the transmission distance. Increasing distance leads to higher beam spreading. However, the spot size of the received signal remains stable up to 300 m, and the atmospheric turbulence leads to negligible effects.

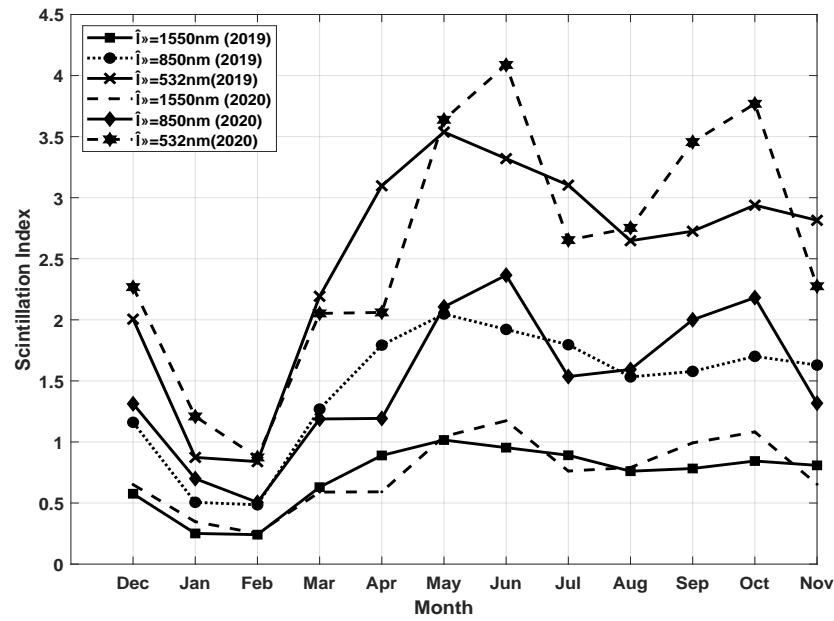


Figure 6. Comparison of Scintillation Index for Different Wavelengths at L = 1000 m.

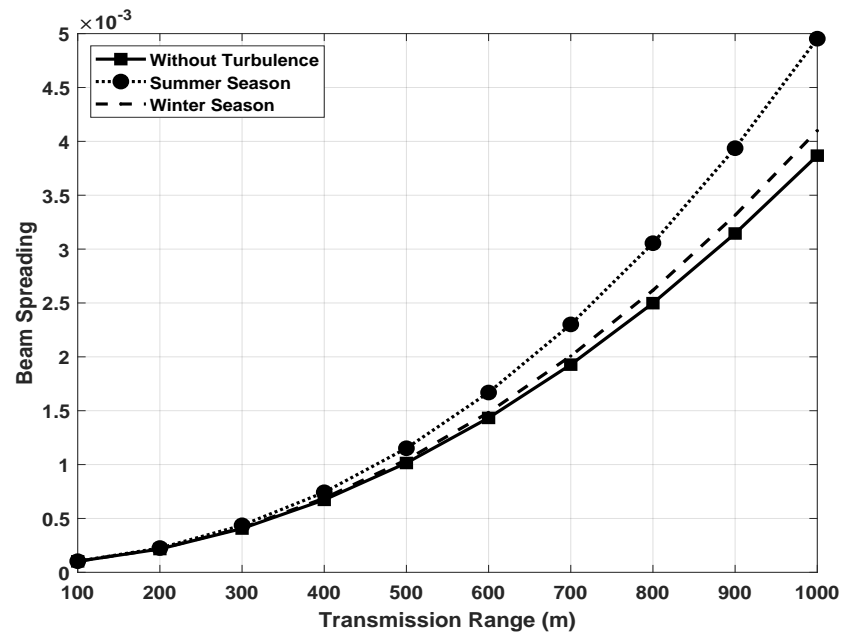


Figure 7. Comparison of the Beam Spreading for Different Transmission Distances.

The BER of transmission depends on the average received power and scintillation strength. Assuming the target of BER as 10^{-9} , Figure 8 shows that on-off keying (OOK) outperforms higher-order modulation, and it also is a cheap and simple modulation technique, which is the reason that we chose it as the proposed modulation technique. Figure 9 illustrates the validation of the employed analytical model against the simulation results. Figures 10 and 11 show the results of a MATLAB simulation conducted to examine the BER performance of the FSO system at different SNRs in both seasons at different propagation distances (from 100 m to 1000 m). The BER performance in winter, with the LN channel used to model the moderate turbulence, and in summer, with the G-G channel used to model the strong turbulence, respectively. Results show that under large propagation distances and strong turbulence, high power is required to achieve the target BER. Moreover, the required SNR is similar for distances ranging from 100 to 300 m in both seasons.

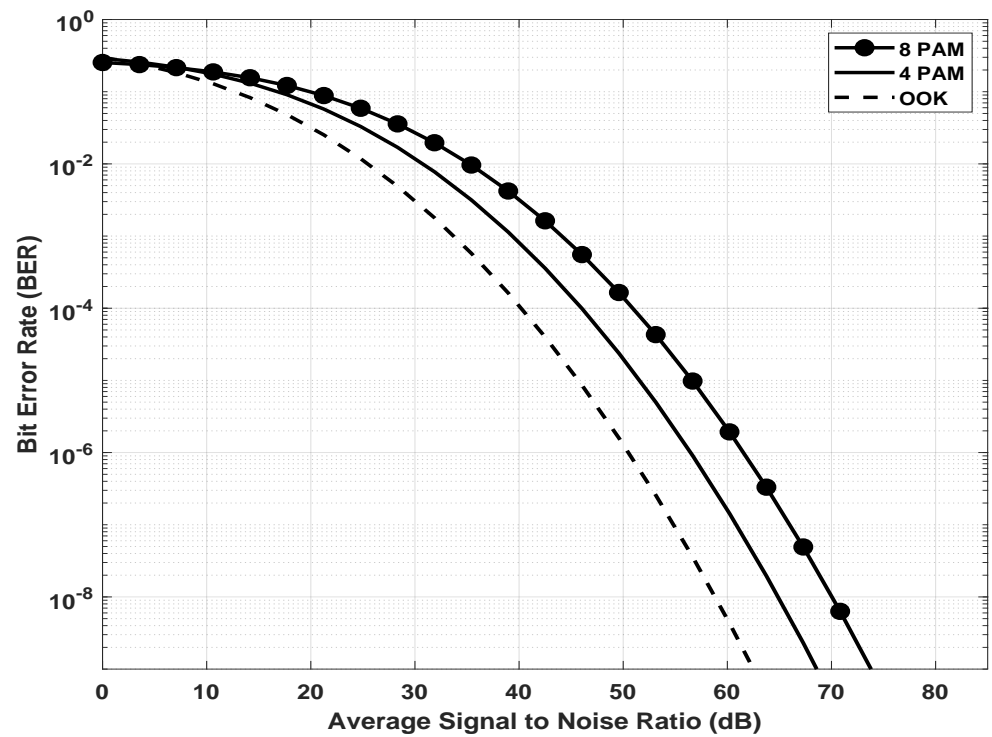


Figure 8. BER Performance for the Proposed System using Different Modulation Order for M-ary PAM in Winter, Modeled using the LN Channel, for 1 km.

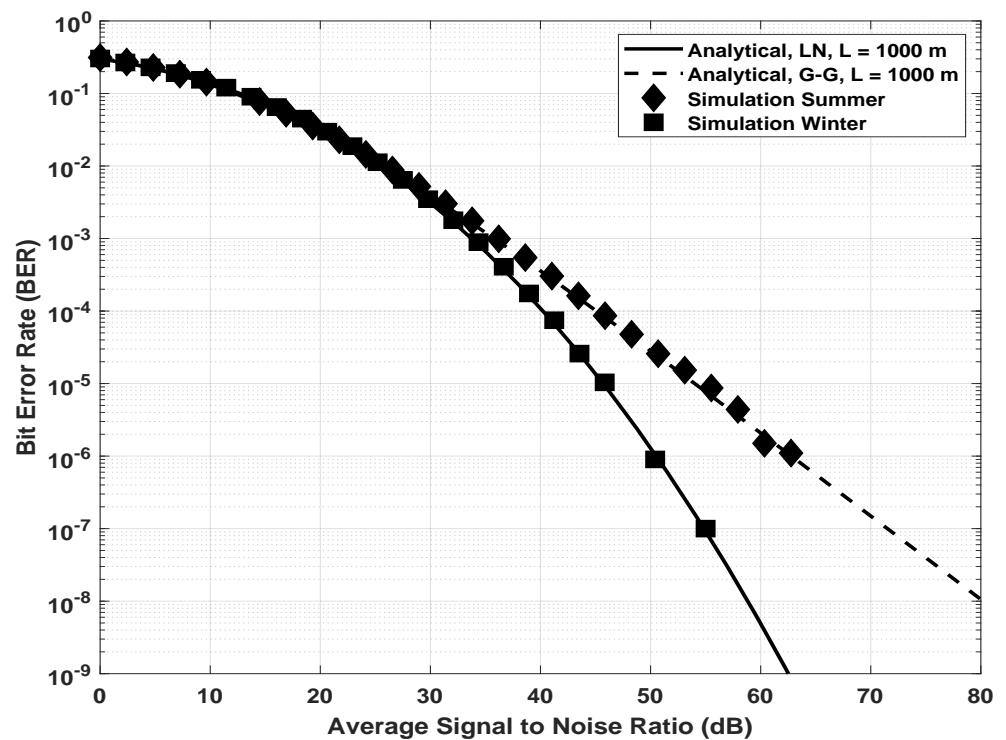


Figure 9. Comparison of BER Determined Analytically and Through Simulations for Gamma-Gamma and Log-Normal Channels.

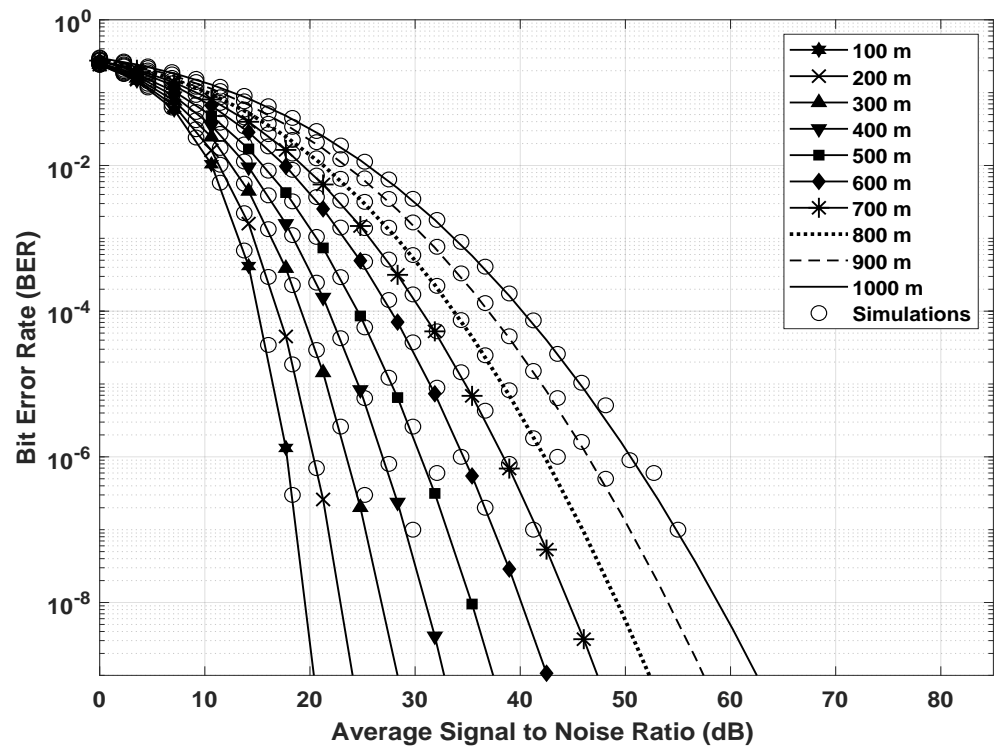


Figure 10. BER Performance for the Proposed System using OOK in Winter, Modeled using the LN Channel, for Different Propagation Distances.

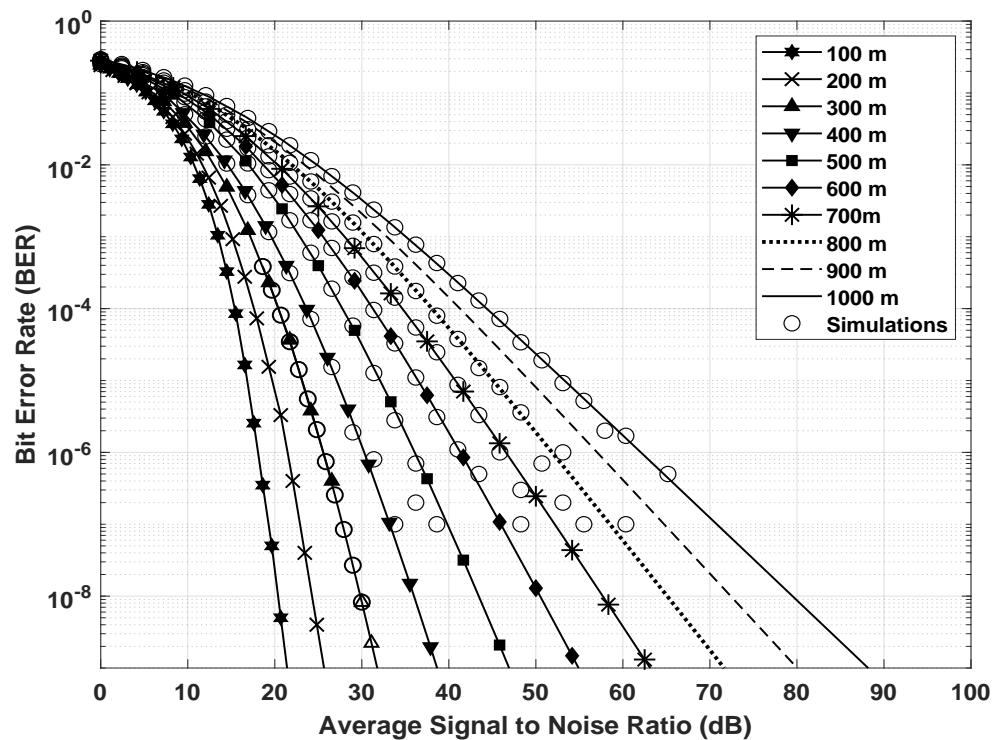


Figure 11. BER Performance for the Proposed System using OOK in Summer, Modeled using the G-G Channel, for Different Propagation Distances.

Figures 12 and 13 show the availability of the proposed system for winter and summer, respectively. Results show that to achieve availability of 99.9 %, a power margin of 9 dB and 17.38 dB must be achieved for winter and summer, respectively.

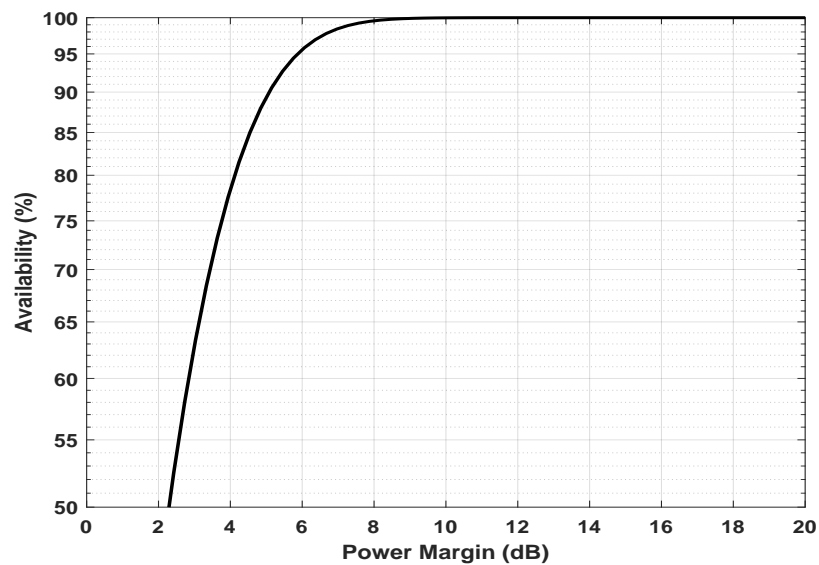


Figure 12. Proposed System Winter Availability.

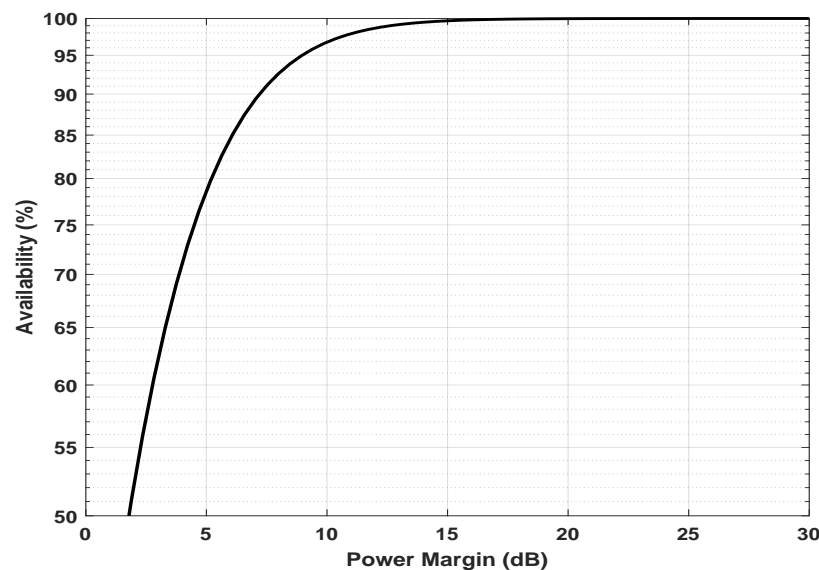


Figure 13. Proposed System Summer Availability.

8. Conclusions

The effect of atmospheric turbulence on FSO communication for NEOM, a smart city envisioned in Saudi Arabia, was examined using daily meteorological data. The FSO link performance, in terms of the SNR, BER, and link availability, was simulated. The results show that in the winter and summer seasons, the atmospheric turbulence is moderate and strong, respectively. Furthermore, the high temperature in summer and relatively high wind speed in winter are the two major weather parameters affecting the FSO performance. Therefore, these factors must be considered during the installation and operation of FSO communication links. Furthermore, it shows that OOK outperforms higher-order modulation PAM. The OOK modulation is a cheap and simple technique which makes it a recommended modulation technique for the considered scenario. Moreover, the atmospheric turbulence exerts a negligible effect at transmission distances less than 300 m. The results indicate that at larger propagation distances, a higher SNR is required to achieve the target BER of 10^{-9} . They shows also that to achieve 99% link availability, the required power margin in summer is about 8 dB more than in winter. Finally, the study shows the

feasibility of FSO in MEOM city where it can be used for applications such as last access and milestone communication solution, Fiber Optic Back-Up link and temporary links.

Author Contributions: Conceptualization, A.S.A. and M.A.; methodology, A.S.; software, M.A.; validation, A.A.Y., M.A.U. and A.M.; formal analysis, A.A.Y.; investigation, A.S.A.; resources, A.S.A.; data curation, A.A.Y.; writing—original draft preparation, A.A.Y.; writing—review and editing, M.A. and A.S.A.; visualization, A.A.; supervision, A.M. and M.A.U.; project administration, A.M.; funding acquisition, A.S.A. All authors have read and agreed to the published version of the manuscript.

Funding: The authors extend their appreciation to the the Deanship of Scientific Research at University of Tabuk for funding this work through Research Group RGP-S-1441-0148.

Institutional Review Board Statement: Not applicable.

Informed Consent Statement: Not applicable.

Data Availability Statement: Not applicable.

Acknowledgments: The authors extend their appreciation to the Saudi National Center for Meteorology for providing weather data for the study.

Conflicts of Interest: The authors declare no conflict of interest. The sponsors had no role in the design, execution, interpretation, or writing of the study.

References

- Klohe, K.; Koudou, B.G.; Fenwick, A.; Fleming, F.; Garba, A.; Gouvras, A.; Harding-Esch, E.M.; Knopp, S.; Molyneux, D.; D'Souza, S.; et al. A Systematic Literature Review of Schistosomiasis in Urban and Peri-Urban Settings. *PLOS Negl. Trop. Dis.* **2021**, *15*, e0008995. [CrossRef]
- Tabane, S.M.N.E.; Zuva, T. Survey of Smart City Initiatives Towards Urbanization. In Proceedings of the 2016 Third International Conference on Advances in Computing and Communication Engineering (ICACCE) 2016, Durban, South Africa, 28–29 November 2019.
- Tan, S.Y.; Taeihagh, A. Smart City Governance in Developing Countries: A Systematic Literature Review. *Sustainability* **2020**, *12*, 899. [CrossRef]
- Wenge, R.; Zhang, X.; Dave, C.; Chao, L.; Hao, S. Smart City Architecture: A Technology Guide for Implementation and Design Challenges. *China Commun.* **2014**, *11*, 56–69. [CrossRef]
- UN-Habitat Core Team and Contributors. Saudi Cities Report 2019. *Ministry of Municipal and Rural Affairs*. Available online: <https://unhabitat.org/sites/default/files/2020/05/Saudi-City-report-english.pdf> (accessed on 1 January 2022).
- Doheim, R.M.; Farag, A.A.; Badawi, S. Smart City Vision and Practices Across the Kingdom of Saudi Arabia A Review. In *Smart Cities: Issues and Challenges*; Elsevier: Amsterdam, The Netherlands, 2019; pp. 309–332.
- Farag, A.A. The Story of NEOM City: Opportunities and Challenges. In *New Cities and Community Extensions in Egypt and the Middle East*; Springer: Berlin/Heidelberg, Germany, 2019; pp. 35–49.
- Alotaibi, D.M.; Akrami, M.; Dibaj, M.; Javadi, A.A. Smart Energy Solution for An Optimised Sustainable Hospital in the Green City of NEOM. *Sustain. Energy Technol. Assess.* **2019**, *35*, 32–40. [CrossRef]
- Al-Gasawneh, J.A.; Al-Adamat, A.M. The Relationship between Perceived Destination Image, Social Media Interaction and Travel Intentions Relating to NEOM City. *Acad. Strateg. Manag. J.* **2020**, *19*, 1–12.
- Salameh, T.; Sayed, E.T.; Abdelkareem, M.A.; Olabi, A.G.; Rezk, H. Optimal Selection and Management of Hybrid Renewable Energy System: NEOM City as A case Study. *Energy Convers. Manag.* **2021**, *244*, 114434. [CrossRef]
- Alqahtani, N.; Balta-Ozkan, N. Assessment of Rooftop Solar P]ower Generation to Meet Residential Loads in the City of NEOM, Saudi Arabia. *Energies* **2021**, *14*, 3805 [CrossRef]
- Papagiannopoulos, N.; Raitsos, D.E.; Krokos, G.; Gittings, J.A.; Brewin, R.J.W.; Papadopoulos, V.P.; Pavlidou, A.; Selmes, N.; Groom, S.; Hoteit, I. Phytoplankton Biomass and the Hydrodynamic Regime in NEOM, Red Sea. *Remote Sens.* **2021**, *13*, 2082. [CrossRef]
- Balalaa, M.S.; Mabrouk, A.B.; Abdessalem, H. A wavelet-based Method for the Impact of Social Media on the Economic Situation: The Saudi Arabia 2030-vision Case. *Mathematics* **2021**, *9*, 1117. [CrossRef]
- Rezk, H.; Alghassab, M.; Ziedan, H. An Optimal Sizing of Stand-Alone Hybrid PV-fuel Cell-Battery to Desalinate Seawater at Saudi NEOM C. *Processes* **2020**, *8*, 382. [CrossRef]
- Boubakri, W.; Abdallah, W.; Boudriga, N. An Optical Wireless Communication based 5G Architecture to Enable Smart City Applications. In Proceedings of the 20th International Conference on Transparent Optical Networks (ICTON) 2018, Bucharest, Romania, 1–5 July 2018.
- Miladić-Tešić, S.D.; Marković, G.Z.; Nonković, N.P. Optical Technologies in Support of the Smart Ccity Concept. *Tehnika* **2020**, *75*, 209–215. [CrossRef]

17. NEOM Launches Infrastructure Work for the World's Leading Cognitive Cities in an Agreement with STC. Available online: <https://www.prnewswire.com/news-releases/neom-launches-infrastructure-work-for-the-worlds-leading-cognitive-cities-in-an-agreement-with-stc-301100431.html> (accessed on 5 October 2021).
18. Aleksic, S. A Survey on Optical Technologies for IoT, Smart Industry, and Smart Infrastructures. *J. Sens. Actuator Netw.* **2019**, *8*, 47. [CrossRef]
19. Abdallah, W.; Boudriga, N. Enabling 5G Wireless Access using Li-Fi Technology: An OFDM based Approach. In Proceedings of the 18th International Conference on Transparent Optical Networks (ICTON) 2016, Trento, Italy, 10–14 July 2016.
20. Gupta, A.; Anand, P.; Khajuria, R.; Bhagat, S.; Jha, R.K. A Survey of Free Space Optical Communication Network Channel over Optical Fiber Cable Communication. *Int. J. Comput. Appl.* **2014**, *105*, 32–36.
21. Harboe, P.B.; Souza, J. Free Space Optical Communication Systems Afeasibility Study for Deployment in Brazil. *J. Microwaves, Optoelectron. Electromagn. Appl. (JMoe)* **2004**, *3*, 58–66.
22. Alma, H.; Al-Khateeb, W. Effect of Weather Conditions on Quality of Free Space Optics Links (with Focus on Malaysia). In Proceedings of the 2008 International Conference on Computer and Communication Engineering, Kuala Lumpur, Malaysia, 13–15 May 2008; pp. 1206–1210.
23. Rouissat, M.; Borsali, A.R.; Chikh-Bled, M.E. Free Space Optical Channel Characterization and Modeling with Focus on Algeria Weather Conditions. *Int. J. Comput. Netw. Inf. Secur.* **2012**, *4*, 17. [CrossRef]
24. Twati, M.O.; Badi, M.M.; Adam, A.F. Analysis of Rain Effects on Free Space Optics based on Data Measured in the Libyan Climate. *Int. J. Inf. Electron. Eng.* **2014**, *4*, 469–472. [CrossRef]
25. Mohale, J.; Handura, M.R.; Olwal, T.O.; Nyirenda, C.N. Feasibility Study of Free-Space Optical Communication for South Africa. *Opt. Eng.* **2016**, *55*, 056108 [CrossRef]
26. Sultana, M.; Barua, A.; Akhtar, J.; Reja, M.I. Performance Investigation of OFDM-FSO System under Diverse Weather Conditions of Bangladesh. *Int. J. Electr. Comput. Eng.* **2018**, *8*, 3722–3731. [CrossRef]
27. Yasir, S.M.; Abas, N.; Saleem, M.S. Performance Analysis of 10Gbps FSO Communication Link Under Suspended Dust and Rain Conditions in Lahore, Pakistan. *Nonlinear Opt. Quantum Opt. Concepts Mod. Opt.* **2019**, *50*, 4.
28. Algamal, A.A.; Fayed, H.A.; Mahmoud, M.; Aly, M.H. Reliable FSO System Performance Matching Multi-Level Customer needs in Alexandria City, Egypt, Climate: Sandstorm Impact with Pointing Error. *Opt. Quantum Electron.* **2020**, *52*, 349. [CrossRef]
29. Tofsted, D.H.; O'Brien, S.G.; Vaucher, G.T. *An Atmospheric Turbulence Profile Model for Use in Army Wargaming Applications I*; Army Research Lab White Sands Missile Range NM Computational and Information; Defense Technical Information Center: Fort Belvoir, VA, USA, 2006.
30. Altowij, K.S.; Alkholidi, A.; Hamam, H. Effect of Clear Atmospheric Turbulence on Quality of Free Space Optical Communications in Yemen. *Front. Optoelectron. China* **2010**, *3*, 423–428. [CrossRef]
31. Shaikh, M.N.; Waqas, A.; Chowdhry, B.S.; Umrani, F.A. Performance and Analysis of FSO Link Availability under Different Weather Conditions in Pakistan. *J. Inst. Electr. Electron. Eng.* **2012**, *76*.
32. Chiyaba, T.K. Analysing the Effect of Visibility and Scintillation on Free Space Optical Communication: A Case of Dodoma and Dar ES Salaam, Tanzania. Ph.D. Thesis, The University of Dodoma, Dodoma, Tanzania, 2018.
33. Garlinska, M.; Pregowska, A.; Masztalerz, K.; Osial, M. From Mirrors to Free-Space Optical Communication—Historical Aspects in Data Transmission. *Future Internet* **2020**, *12*, 179. [CrossRef]
34. Pang, X.; Ozolins, O.; Zhang, L.; Schatz, R.; Udalcovs, A.; Yu, X.; Jacobsen, G.; Popov, S.; Chen, J.; Lourduoss, S. Free-Space Communications Enabled by Quantum Cascade Lasers. *Phys. Status Solidi A* **2021**, *218*, 2000407. [CrossRef]
35. Spitz, O.; Didier, P.; Durupt, L.; Baranov, A.N.; Cerutti, L.; Grillot, F. Free-Space Communication with Directly Modulated Mid-Infrared Quantum Cascade Devices. *IEEE J. Sel. Top. Quantum Electron.* **2022**, *28*, 1–9. [CrossRef]
36. Lionis, A.; Peppas, K.; Nistazakis, H.E.; Tsigopoulos, A.D.; Cohn, K. Experimental performance analysis of an optical communication channel over maritime environmen. *Electronics* **2020**, *9*, 1109. [CrossRef]
37. Garlinska, M.; Pregowska, A.; Gutowska, I.; Osial, M.; Szczepanski, J. Experimental Study of the Free Space Optics Communication System Operating in the 8–12 μm Spectral Range. *Electronic* **2021**, *10*, 875. [CrossRef]
38. Wang, Y.; Xu, H.; Li, D.; Wang, R.; Jin, C.; Yin, X.Y.; Gao, S.; Mu, Q.; Zuan, L.; Cao, Z. Performance analysis of an adaptive optics system for free-space optics communication through atmospheric turbulence. *Sci. Rep.* **2018**, *8*, 1124. [CrossRef]
39. Alkholidi, A.; Altowij, K. Effect of Clear Atmospheric Turbulence on Quality of Free space Optical Communications in Western Asia. *Opt. Commun. Syst.* **2012**, *1*, 41–72.
40. Raj, A.A.B.; Selvi, J.A.V.; Durairaj, S. Comparison of Different Models for Ground-Level Atmospheric Turbulence Strength (C_n^2) Prediction with A New Model According to Local Weather Data for FSO Applications. *Appl. Opt.* **2015**, *54*, 802–815.
41. Wilcox, C.C.; Restaino, S.R. *A New Method of Generating Atmospheric Turbulence with A Liquid Crystal Sspatial Light Modulator; THI Sone Is: A Chapter in New Development in Liquid Crystals*; InTech: Toyama, Toyama, 2009; ISBN 978-953-307-015-5.
42. Sadot, D.; Kopeika, N.S. Forecasting Optical Turbulence Strength on the Basis of Macroscale Meteorology and Aerosols: Models and Validation. *Opt. Eng.* **1992**, *31*, 200–212. [CrossRef]
43. Bendersky, S.; Kopeika, N.S.; Blaunstein, N. Atmospheric Optical Turbulence over Land in Middle East Coastal Environments: Prediction Modeling and Measurements. *Appl. Opt.* **2004**, *43*, 4070–4079. [CrossRef] [PubMed]
44. Lionis, A.; Peppas, K.; Nistazakis, H.E.; Tsigopoulos, A.; Cohn, K. Statistical Modeling of Received Signal Strength for An FSO Link over Maritime Environment. *Opt. Commun.* **2021**, *489*, 126858. [CrossRef]

45. Wang, H.; Li, B.; Wu, X.; Liu, C.; Hu, Z.; Xu, P. Prediction Model of Atmospheric Refractive Index Structure Parameter in Coastal Area. *J. Mod. Opt.* **2015**, *62*, 1336–1346. [[CrossRef](#)]
46. Bendersky, S.; Lilos, E.; Kopeika, N.S.; Blaunstein, N. Modeling and Measurements of Near-Ground Atmospheric Optical Turbulence According to Weather for Middle East Environments. In Proceedings of the SPIE 5612, Electro-Optical and Infrared Systems: Technology and Applications, London, UK, 6 December 2004. [[CrossRef](#)]
47. Jellen, C.; Nelson, C.; Brownell, C.; Burkhardt, J.; Oakley, M. Measurement and Analysis of Atmospheric Optical Turbulence in a Near-Maritime Environment. *IOP SciNotes* **2020**, *1*, 024006. [[CrossRef](#)]
48. Porrás, R.B. Exponentiated Weibull Fading Channel Model in Free-Space Optical Communications Under Atmospheric Turbulence. Ph.D. Dissertation, Universitat Politècnica de Catalunya, Barcelona, Spain, 2013.
49. Farid, A.A.; Hranilovic, S. Outage Capacity Optimization for Free-Space Optical Links with Pointing Errors. *J. Light. Technol.* **2007**, *25*, 1702–1710. [[CrossRef](#)]
50. Abaza, M.; Mesleh, R.; Mansour, A.; Aggoune, E.-H.M. Relay Selection for Full-Duplex FSO Relays over Turbulent Channels. In Proceedings of the 16TH IEEE International Symposium on Signal Processing and Information Technology (ISSP 2016), Limassol, Cyprus, 12–14 December 2016.
51. Saud, M.M.A. *Sustainable Land Management for NEOM Region*; Springer: Berlin/Heidelberg, Germany, 2020.
52. Zhangy, M.; Tang, X.; Lin, B.; Ghassemlooy, Z.; Wei, Y. Analysis of Rytov Variance in Free Space Optical Communication under the Weak Turbulence. In Proceedings of the 16th International Conference on Optical Communications and Networks (ICOON), Wuzhen, China, 7–10 August 2017.
53. Moradi, H.; Refai, H.H.; LoPresti, P.G. Switched Diversity Approach for Multireceiving Optical Wireless Systems. *J. Appl. Opt.* **2011**, *50*, 5606–5614. [[CrossRef](#)]
54. Youssef, A.A.; Abaza, M.; Alatawi, A.S. LDPC Decoding Techniques for Free-Space Optical Communications. *IEEE Access* **2021**, *9*, 133510–133519. [[CrossRef](#)]
55. Abaza, M.; Mesleh, R.; Mansour, A.; Aggoune, H.M. Performance Analysis of MISO Multi-Hop FSO Links over Log-Normal Channels with Fog and Beam Divergence Attenuations. *Opt. Commun.* **2015**, *334*, 247–252. [[CrossRef](#)]
56. Abramowitz, M.; Stegun, I.A.; Romer, R.H. *Handbook of Mathematical Functions with Formulas, Graphs, and Mathematical Tables*; Dover Publication: Mineola, NY, USA, 1988.
57. Kiasaleh, K. Performance of APD-based, PPM Free-Space Optical Communication Systems in Atmospheric Turbulence. *IEEE Trans. Commun.* **2005**, *53*, 1455–1461. [[CrossRef](#)]
58. Safari, M.; Uysal, M. Relay-Assisted Free-Space Optical Communication. *IEEE Trans. Wirel. Commun.* **2008**, *7*, 5441–5449. [[CrossRef](#)]
59. Xu, Z.; Xu, G.; Zheng, Z. BER and Channel Capacity Performance of An FSO Communication System over Atmospheric Turbulence with Different Types of Noise. *Sensors* **2021**, *21*, 3454. [[CrossRef](#)] [[PubMed](#)]
60. Chatzidiamantis, N.D.; Michalopoulos, D.S.; Kriezis, E.E.; Karagiannidis, G.K.; Schober, R. Relay Selection Protocols for Relay-Assisted Free-Space Optical Systems. *J. Opt. Commun. Netw.* **2013**, *5*, 92–103. [[CrossRef](#)]
61. Zhangy, M.; Tang, X.; Lin, B.; Ghassemlooy, Z.; Wei, Y. Experimental setup to validate the effects of major environmental parameters on the performance of FSO communication link in Qatar. *Appl. Sci.* **2018**, *8*, 2599.
62. Ali, M.A.; Ali, A. Atmospheric turbulence effect on free space optical communications. *Int. J. Emerg. Technol. Comput. Appl. Sci.* **2013**, *5*, 345–351.
63. Ali, R.N.; Jassim, J.M.; Jasim, K.M.; Jawad, M.K. Experimental study of clear atmospheric turbulence effects on laser beam spreading in free space. *Int. J. Appl. Eng. Res.* **2017**, *12*, 14789–14796.